

Accepted Manuscript

Research paper

Effective delivery of hydrophobic drugs to breast (MCF-7) and Liver (HepG2) cancer cells: A detailed investigation using Cytotoxicity assays, fluorescence imaging and flow cytometry

Danushika C. Manatunga, Rohini M. de Silva, K.M. Nalin de Silva, Gathsaurie Neelika Malavige, Dulharie T. Wijeratne, Gareth R. Williams, Chanika D. Jayasinghe, Preethi V. Udagama



PII: S0939-6411(17)31346-2
DOI: <https://doi.org/10.1016/j.ejpb.2018.04.001>
Reference: EJPB 12731

To appear in: *European Journal of Pharmaceutics and Biopharmaceutics*

Received Date: 22 November 2017
Revised Date: 30 March 2018
Accepted Date: 2 April 2018

Please cite this article as: D.C. Manatunga, R.M. de Silva, K.M. Nalin de Silva, G. Neelika Malavige, D.T. Wijeratne, G.R. Williams, C.D. Jayasinghe, P.V. Udagama, Effective delivery of hydrophobic drugs to breast (MCF-7) and Liver (HepG2) cancer cells: A detailed investigation using Cytotoxicity assays, fluorescence imaging and flow cytometry, *European Journal of Pharmaceutics and Biopharmaceutics* (2018), doi: <https://doi.org/10.1016/j.ejpb.2018.04.001>

This is a PDF file of an unedited manuscript that has been accepted for publication. As a service to our customers we are providing this early version of the manuscript. The manuscript will undergo copyediting, typesetting, and review of the resulting proof before it is published in its final form. Please note that during the production process errors may be discovered which could affect the content, and all legal disclaimers that apply to the journal pertain.

Effective delivery of hydrophobic drugs to breast (MCF-7) and Liver (HepG2) cancer cells: A detailed investigation using Cytotoxicity assays, fluorescence imaging and flow cytometry

Danushika C. Manatunga^a, Rohini M. de Silva^{a*}, K. M. Nalin de Silva^{a,b}, Gathsaurie Neelika Malavige^c, Dulharie T. Wijeratne^c, Gareth R. Williams^d, Chanika D. Jayasinghe^e, Preethi V. Udagama^e

a. Department of Chemistry, University of Colombo, Colombo 00300, Sri Lanka. Email:rohini@chem.cmb.ac.lk

b. Sri Lanka Institute of Nanotechnology (SLINTEC), Nanotechnology & Science Park, Mahenwatte, Pitipana, Homagama 10206, Sri Lanka

c. Center for Dengue Research, Department of Microbiology, Faculty of Medical Sciences, University of Sri Jayawardenepura, 10250, Sri Lanka

d. UCL School of Pharmacy, University College London, 29–39 Brunswick Square, London WC1N 1AX, United Kingdom

e. Department of Zoology, University of Colombo, Colombo 00300, Sri Lanka.

Abstract

This study aimed to develop a drug carrier system consisting of a polymer containing hydroxyapatite (HAp) shell and a magnetic core of iron oxide nanoparticles. Doxorubicin and/or curcumin were loaded into the carrier via a simple diffusion deposition approach, with encapsulation efficiencies (EE) for curcumin and doxorubicin of $93.03 \pm 0.3\%$ and $97.37 \pm 0.12\%$ respectively. The co-loading of curcumin and doxorubicin led to a total EE of $76.02 \pm 0.48\%$. Release studies were carried out at pH 7.4 and 5.3, and revealed higher release was at pH 5.3 expressing the potential application in tumor microenvironments. Cytotoxicity assays, fluorescence imaging and flow cytometry showed the formulations could effectively inhibit the growth of MCF-7 and HEpG2 cancer cells, being more potent than the free drug molecules both in dose and time dependent manner. Additionally, hemolysis tests and cytotoxicity evaluations determined the drug-loaded carriers to be non-toxic towards non-cancerous cells. These formulations thus have great potential in the development of new cancer therapeutics.

Key words: Doxorubicin, curcumin, Hydroxyapatite, Iron oxide, MCF7, HEpG2

1 Introduction

Regardless to the numerous advancements in the field of cancer treatment, the occurrence [1],[2] and death due to breast and hepatocellular carcinoma (HCC) are keep on rising over the years[1],[3] where breast cancer and HCC would account for 40, 610 deaths in US and 600, 000 deaths worldwide respectively[3].

For decades, chemotherapy has been the mainstay treatment for both breast and liver cancer [4]. Indeed, in HCC when the patient is diagnosed at late stage, chemotherapy becomes the only available option [5]. Doxorubicin has been identified as the most effective chemotherapeutic for many cancer types including breast cancer and HCC, despite its having many unavoidable serious side effects [6], [7]. Adverse effects mainly originate owing to high plasma levels of free doxorubicin, due to the use of high doses systemically [8]. Improved targeting is thus required.

To achieve this goal, many strategies, such as incorporation into a carrier or combining doxorubicin synergistically with another compound to reduce the toxicity have been employed [9]. Many selective and passive delivery vehicles have been prepared using nanotechnology [9], with the PEGylated liposomal formulation of doxorubicin (Doxil®) being the first to receive clinical approval. Doxil shows increased circulation times and more rapid uptake into tumor cells than standard doxorubicin formulations, thereby reducing the cardiotoxicity, and other side effects [8], [10].

A range of more advanced liposomal formulations such as those which are temperature sensitive, enzyme sensitive, light sensitive or functionalized with a targeting antibody [11] have also been fabricated for the purpose of doxorubicin delivery [10]. In addition, alternate systems copolymer micelles [12], hydroxyapatite nanoparticles [13],[14], hydrogels[15] and polymer-lipid hybrid nanostructures[16] has also of main interest. In many of these instances, while the formulations

reduce the toxicity exerted on normal cells their anti-cancer properties are only slightly improved [17].

Curcumin, a well-known Asian spice is a polyphenolic compound reported to have anti-carcinogenic properties, along with many other beneficial effects [9],[18],[19]. Importantly it is much safer as a drug with no dose limiting toxicity [20]. The application of curcumin as an anti-cancer agent has been limited due to its low aqueous solubility leading to poor bioavailability, short half-life, and rapid excretion [19],[21]. As for doxorubicin, these issues have been ameliorated in various studies via loading curcumin in a polymer drug carriers, lipid carriers, dendrimers, liposomes, nanogels, micelles, microspheres, cyclodextrins, and inorganic nanoparticles [19],[22],[23]. Because curcumin can control and induce cell apoptosis, there may be benefits in applying it in combination therapy with chemotherapeutics like doxorubicin [24],[25].

Hydroxyapatite nanoparticles (HAp) are well known drug delivery vehicles as they offer high drug pay loads, pH sensitivity and controlled release of incorporated active ingredients [19],[26]. On the otherhand, to reduce off-target effects, the nanoparticles like iron oxide nanoparticles (IONPs) have been used as delivery vehicles to achieve magnetic targeting to tumor cells [18].

The combination of HAp with IONPs could be beneficial because it could enhance the biocompatibility and also the drug loading ability of magnetic nanoparticles which will ultimately provide the targeted delivery option [19],[27].

However, in our previous studies it has been shown that a strong interaction in between HAp and IONPs could be built up, if a polysaccharide like sodium alginate (NaAlg) is used as a linker [28].

The use of magnetic HAp particles has received some attention for the treatment of cancer [21],[29],[30]. There is no work to date on the use of HAp- NaAlg-IONP composites for the treatment of breast or liver cancer. Therefore, in this study we develop a novel drug carrier which can perform targeted, pH responsive and sustained delivery of doxorubicin, curcumin or both together on cancer cells (breast/ liver). For this purpose, hydroxyapatite was deposited on sodium

alginate decorated iron oxide nanoparticles, then loaded with the respective drugs and assessed for their activity on two different cancer cell lines (MCF-7 and HEpG2).

2. Experimental

2.1. Materials and methods

Curcumin (>98.0%, HPLC), doxorubicin hydrochloride (Dox- HCl, 98.0-102.0% (HPLC)), calcium nitrate tetra hydrate ($\text{Ca}(\text{NO}_3)_2 \cdot 4\text{H}_2\text{O}$, 99%, ACS), diammonium hydrogen phosphate ($(\text{NH}_4)_2\text{HPO}_4$, > 99.0%), ammonium iron(II) sulfate hexahydrate ($(\text{NH}_4)_2\text{Fe}(\text{SO}_4)_2 \cdot 6\text{H}_2\text{O}$, 99.0%, ACS), ammonium iron(III) sulfate dodecahydrate ($\text{NH}_4\text{Fe}(\text{SO}_4)_2 \cdot 12 \text{H}_2\text{O}$, 99.0%, ACS), ethanol (EtOH, > 99.8%, HPLC), dichloromethane (CH_2Cl_2 anhydrous, > 99.8%), alginic acid sodium salt (NaAlg, low viscosity), Cetyltrimethyl ammonium bromide (CTAB, > 98%) and TWEEN® 80 (Viscous liquid), ammonium hydroxide solution (puriss. p.a., 25% NH_3 in H_2O) were used as main reagents and purchased from Sigma Aldrich, Bangalore, India. Polyethyleneglycol 200 (PEG 200) was purchased from Merck Millipore Corporation, Darmstadt, Germany for the preparation of surfactant coated IONPs. Snakeskin dialysis tubing (MWCO 3.5 kDa) was purchased from Thermo Fisher, Bangalore, India. Ultrapure deionized water was used for all the experiments.

2.2. Cell lines, animals, and reagents

The MCF-7 breast carcinoma and HEpG2 hepatocellular carcinoma cell lines were purchased from ECACC (Salisbury, UK). MCF-7 cells were cultured in DMEM medium (Gibco, USA) containing 10% fetal bovine serum (FBS, Gibco, USA), 100 U/mL of penicillin and 100 $\mu\text{g}/\text{mL}$ of streptomycin, 1% 200 mM L-glutamine (Gibco, USA) and 1% non-essential amino acids (NEAA, 100x, Gibco, USA) at 37 °C in a humidified 5% CO_2 atmosphere. Similarly, HEpG2 cells were cultured in complete RPMI 1640 medium at 37 °C in a humidified 5% CO_2 atmosphere. The passaging of the cell lines was carried out 2-3 times per week using 0.05% Trypsin EDTA (Gibco,

USA). The African Green monkey kidney epithelial cell line Vero (ATCC, USA) was grown in complete DMEM with passage carried out in every 3-4 days using 0.05% Trypsin EDTA.

Male Wistar rats of weight 150-200 g were obtained from the rat house of the Zoology Department, University of Colombo. The animals were housed in plastic cages under standard conditions (temperature 28-31°C; approximately 12 hours' natural light per day, relative humidity 50-55%). The animals were fed with food pellets (Master Feed Ltd, Colombo, Sri Lanka) and provided with drinking water *ad libitum*. Animal experiments were ethically approved by the Institute of Biology of Sri Lanka (Registration No: ERC IOBSL140 02 16).

2.3 Preparation of NaAlg-hydroxyapatite-IONPs (ALG-HI)

The co-precipitation technique was followed for the synthesis of the drug carrier as reported in our previous work [28]. Polyethylene glycol (PEG) coated IONPs were synthesized using 0.1 M iron precursor solutions (ammonium iron (II) sulfate hexahydrate $((\text{NH}_4)_2\text{Fe}(\text{SO}_4)_2 \cdot 6\text{H}_2\text{O})$, ammonium iron (III) sulfate dodecahydrate $(\text{NH}_4\text{Fe}(\text{SO}_4)_2 \cdot 12 \text{H}_2\text{O})$ where the obtained IONPs were later functionalized with sodium alginate polymer molecules. These alginate functionalized IONPs were then added to a 0.25 M $\text{Ca}(\text{NO}_3)_2$ solution maintained at pH 8 under vigorous stirring. The pH was adjusted to 9 and a solution of $(\text{NH}_4)_2\text{HPO}_4$ was introduced slowly to obtain ALG-HI nanocomposite [28]. The resultant black brown suspension was separated, washed and stored at 4°C until further use.

2.4. Drug loading

The loading of curcumin to ALG-HI was performed via a wet milling approach in accordance with a previous report [28]. The obtained yellow brown color suspension (CR-ALG-HI) was separated, washed and stored at 4°C for until further use. For the loading of doxorubicin, 33.33 mL of a 50 ppm aqueous doxorubicin solution was added immediately to a 0.06g/mL ALG-HI suspension and provided with stirring at 120 rpm and at 37°C for 17 hours. The doxorubicin-loaded nanoparticles were recovered via magnetic separation (DX-ALG-HI). The amount of loaded doxorubicin was

calculated via fluorescence spectroscopy (HORIBA fluorescence spectrophotometer; $\lambda_{\text{excitation}}$ 467 nm and $\lambda_{\text{emission}}$ 589 nm) [31]. In order to load both curcumin and doxorubicin, curcumin was initially incorporated to the ALG-HI, magnetically separated, and then the nanoparticles were further incubated with 50 ppm doxorubicin solution (DX.CR-ALG-HI).

2.5. Quantification of the loaded drug content

The amount of curcumin in the NPs was determined via a simple desorption process[28]. A known amount of CUR-ALG was incubated with ethanol under ultrasonic irradiation. Aliquots of the released curcumin were taken periodically replacing with an equal amount of fresh ethanol. The curcumin content in aliquots was determined spectrophotometrically (GENESYS 10S, ThermoFisher Scientific) at 430 nm.

However, the remaining doxorubicin content was measured via fluorescence spectroscopy (HORIBA, Fluorolog, fluorescence spectrophotometer) to calculate the doxorubicin content that has been loaded in to the composite nanoparticle. Based on the loaded drug content the drug loading capacity and encapsulation efficiency[32] were determined.

2.6. Characterization of ALG-HI and the drug loaded systems

The powder X-ray diffraction analysis (PXRD) was performed to determine the crystallographic phase of the synthesized ALG-HI. Samples were subjected to Cu $\kappa\alpha$ radiation at $\lambda = 1.5418 \text{ \AA}$ and the measurements were taken in the 2θ range of 5-75 (Bruker D8 Focus X-ray diffractometer, Germany). Fourier transform infra-red (FR-IR) spectra were recorded on a Vertex 80 instrument (Bruker, Germany). Spectra were collected over the range of 400-4000 cm^{-1} using KBr pellets. Scanning electron microscopy (SEM) was performed on a SU 6600 instrument (Hitachi, Japan) operating at 5.0- 15 kV. Further visualization of the sample was undertaken with the use of transmission electron microscope (TEM, JEM-2010, JEOL, Japan) operating at 80 kV.

Samples were also subjected to X-ray photoelectron spectroscopy (XPS) analysis by NEXUS facility (Newcastle University) in UK. A K-alpha instrument (Thermo Scientific, East Grinstead, UK)

equipped with a monochromated Al K α X-ray source was used with a pass energy of 40 eV and step size of 0.1 eV. Spectra were processed using the CasaXPS software (Casa Software Ltd., Teignmouth, UK) to identify the possible interactions of the drug molecules with the carrier ALG-HI.

2.7. In-vitro release studies

Release studies were carried out using the dialysis method, similar to the previous work by our group [28]. Briefly two PBS buffer solutions at pH 7.4 or 5.3 were prepared and supplemented with 1% (w/w) of Tween 80. A known amount of the drug bound nanoparticles were placed in a dialysis bag (MWCO of 3500) and immersed in the buffer solutions (20 mL) under gentle stirring at 37°C. At specific time intervals, 0.5 ml of the solution was withdrawn and replenished with an equal volume of fresh preheated buffer. These aliquots removed were analyzed for curcumin and doxorubicin as detailed above. The release study was continued until the solution drug concentration reached an equilibrium. All experiments were carried out in triplicate. The following equation (Eq. 1) was used to determine the cumulative drug release percentage [33].

$$\text{Cumulative drug release (\%)} = \frac{\text{Total amount of drug released at a specific point of time}}{\text{Total amount of drug bound to the nanoparticle}} \times 100\% \dots (\text{Eq. 1})$$

2.8. In-vitro cytotoxicity assessment

The in vitro cytotoxicity of the formulations against MCF-7 and HEPG2 cells was determined with the WST-1 cell viability determination assay [34]. Cells were seeded in 96- well plates (Greiner CELLSTAR®, Germany) at a density of 3×10^3 cells/ well overnight [21],[35] in the appropriate media under standard cell culture conditions. They were subsequently treated with a series of different concentrations of the nanoparticles and/or drug loaded nanoparticles dispersed in complete media for 24, 48 and 72 hours and the subsequently the cell viability was detected [36] using WST-1 solution (Abcam, UK). The detailed protocol is given in supplementary information.

2.9. Cellular uptake studies

Cells were first cultured in 8-well chamber slides (Nunc® Lab-Tek® Chamber Slide™, USA) and treated with IC50 concentrations of nanoparticles for 24, 48 and 72 hours. All experiments were performed in triplicate. After each incubation the cells were washed with cold PBS, fixed with 3.7% paraformaldehyde in PBS (VWR, UK) for 15 minutes at room temperature. The fixed cells were washed and treated with 100µg/mL AO/EB (Thermo Fisher Scientific, Life Technologies, Singapore) solution for 10 minutes in the dark [37]. Similarly, for Hoechst staining the fixed cells were washed with 0.1% Triton X in PBS followed by the addition of 5µg/mL Hoechst (Thermo Fisher Scientific, Life Technologies, Singapore) in 0.1% Triton X/PBS and incubated for 15 minutes at room temperature in the dark. After each incubation the stained cells were washed with PBS and a coverslip placed on the slide using a permanent mounting medium[38]. Finally, the samples were visualized under a fluorescence microscope (FSX 100, Olympus, Japan).

2. 10. Flow cytometry

Apoptosis was quantified by flow cytometry using the Annexin V APC (Biolegend- Cat number- 640920) and Zombie green (ZG- Biolegend- Cat number - 423111) double staining protocol [39]. MCF or HEPG2 cells/well were grown in 24 well plates overnight under standard cell culture conditions. On the following day the cells were incubated with the IC50 values of each nanoparticle system for another 18 hours. After the incubation they were washed, trypsinized, detached, stained and analyzed by flow cytometry. Media alone was used as the negative control. To avoid the spectral overlap, single stains of cells with Annexin V and cells with ZG were used as compensation controls at each time of the experiment. The expression of Annexin V and ZG were acquired (Guava easyCyte 12 HT instrument, Merck, Germany equipped with blue Laser (488 nm), red laser (642nm) and violet laser (405nm) and the data were analyzed by FCS express version 4 (denovo software). All experiments were undertaken in triplicated.

2. 11. Hemolysis assay

Hemolysis (rupture of red blood cells- RBCs) was also used as a measure of cytotoxicity evaluation of the nanomaterials[21]. Briefly, rat blood collected into EDTA was centrifuged, rinsed and diluted in PBS. 100 μ l aliquots of the diluted red blood cells were added to 900 μ l of a test solution containing different concentrations (0.01- 160.0 μ g/mL) of the nanoparticles. The samples were next incubated for 2 hours with gentle shaking. RBCs incubated with deionized water and PBS were used as the positive and the negative controls, respectively. After incubation the samples were centrifuged and the absorbance of the supernatant measured at 541 nm using a UV-visible spectrophotometer (ThermoScientific™ GENESYS 10S, India). All samples were tested in triplicate. The following equation was used to obtain the percentage of hemolysis (E.q. 3)[21];

$$\text{Hemolysis (\% of the RBCs)} = \frac{(A_{\text{sample}} - A_{\text{negative control}})}{(A_{\text{positive control}} - A_{\text{negative control}})} \times 100 \% \dots (\text{Eq. 3})$$

Where A_{sample} is the absorbance of the blood of the test sample, $A_{\text{negative control}}$ is the absorbance of the blood with PBS and $A_{\text{positive control}}$ is the absorbance of the blood with water.

2.12. Effect of the formulations on rat bone marrow cells

Myelosuppression is the single most important factor that determines the toxicity in treatment of cancer[40]. The detailed description on obtaining rat bone marrow cells is given in supplementary information. After several washing steps with RPMI, the primary bone marrow cells obtained from sacrificed rats were seeded at a density of $1-9 \times 10^4$ cells/ well in 96 cell well plates in complete RPMI medium, and incubated for 3 hours under standard cell culture conditions. These cells were then treated with a series of different concentration of nanoparticles for 24 hours[41]. Thereafter, cell viability was assessed via the MTT assay protocol[42]. All samples were tested in triplicate in three individual experiments.

2.13. Effect of the formulations on non-cancerous Vero cells

In addition to the effect on cancerous cells, the effect of these bare nanoparticles and drug loaded nanoparticles on a non-cancerous epithelial cell lines such as Vero was also assessed as reported in previous studies[43]. The cells were seeded in 96 well plates and incubated for overnight under

standard cell culture conditions. On the following day they were treated with a series of different concentrations of nanoparticles and incubated for 24 hours before cell viability was assessed via the WST-1 cell viability assessment assay as specified in section 2.8.

2. 14. Statistical analysis

Data are presented as mean \pm SEM. One-way analysis (ANOVA) of variance was used to determine statistical significance of the cumulative release rate and cell viability followed by Tukey—Kramer post-hoc test analysis of variance. P-values < 0.05 were considered statistically significant. All statistical analyses were performed using SPSS version 19 (IBM Corporation, Armonk, NY, USA).

3. Results and discussion

3.1. Synthesis and characterization of drug-loaded nanoparticles

The obtained neat drug carrier was characterized using XRD, FT-IR and SEM analysis and the successful synthesis of ALG-HI can be confirmed as data given in supplementary information (Fig. S1, Fig. S2 and Fig. S3) which were published in our previous report[28].

Fig. 1. displays the FT-IR spectra of the formulations. Fig. 1. a. is the spectra of neat ALG-HI which is compared with the drug loaded systems. In neat curcumin (Fig. 1.b.), the appearance of a sharp band at 3511 cm^{-1} and a broader peak at 3373 cm^{-1} can be attributed to aliphatic -OH groups and phenol -OH groups respectively[19],[35],[44]. When curcumin molecules interacted with the ALG-HI (CR- ALG-HI) (Fig. 1.c.), there is a clear broadening and the reduction of the -OH stretching vibrational bands[45]. Furthermore, the appearance of -CH_2 stretching vibrational bands of CTAB [46] at 2925 cm^{-1} and 2856 cm^{-1} has masked the appearance of the CH stretch of -O-CH_3 of curcumin which could possibly appear at 2946 cm^{-1} [44]. Additionally, the 1374 cm^{-1} and 816 cm^{-1} vibrational bands of neat curcumin (CH deformation of -CH_3 groups and alkene bends)[45] have

shifted to 1395 cm^{-1} and 818 cm^{-1} in the curcumin loaded nanoparticles further providing the evidence of the interaction of curcumin with the nanoparticles. The FT-IR spectra of both neat doxorubicin and DX-ALG-HI are given in Fig. 1. d. and e. Similar observation on the band shifting can be made for DX-ALG-HI (Fig. 1.e.). The -OH stretching band of doxorubicin[47] is visible at 3371 cm^{-1} in DX-ALG-HI, from its position in the neat drug carrier nanoparticle (3141 cm^{-1}). The presence of bands at 1584 cm^{-1} and 1616 cm^{-1} of neat doxorubicin (Fig. 1.d.) can be attributed to the stretching of two carbonyl groups of the anthracyclines [21]. The appearance of an intense band at 1616 cm^{-1} further confirmed the incorporation of doxorubicin molecules in to the nanoparticle in DX-ALG-HI. Moreover, a weak band at 1287 cm^{-1} in the doxorubicin loaded nanoparticle system corresponds to the -C-O-C- stretching vibration of doxorubicin[48].

When both curcumin and doxorubicin were co-loaded to the ALG-HI (DX. CR-ALG-HI) (Fig.1. f), it has become very similar to the CR-ALG-HI. However, the interaction of these drug molecules with the ALG-HI could be further confirmed by the XPS given in supplementary information.

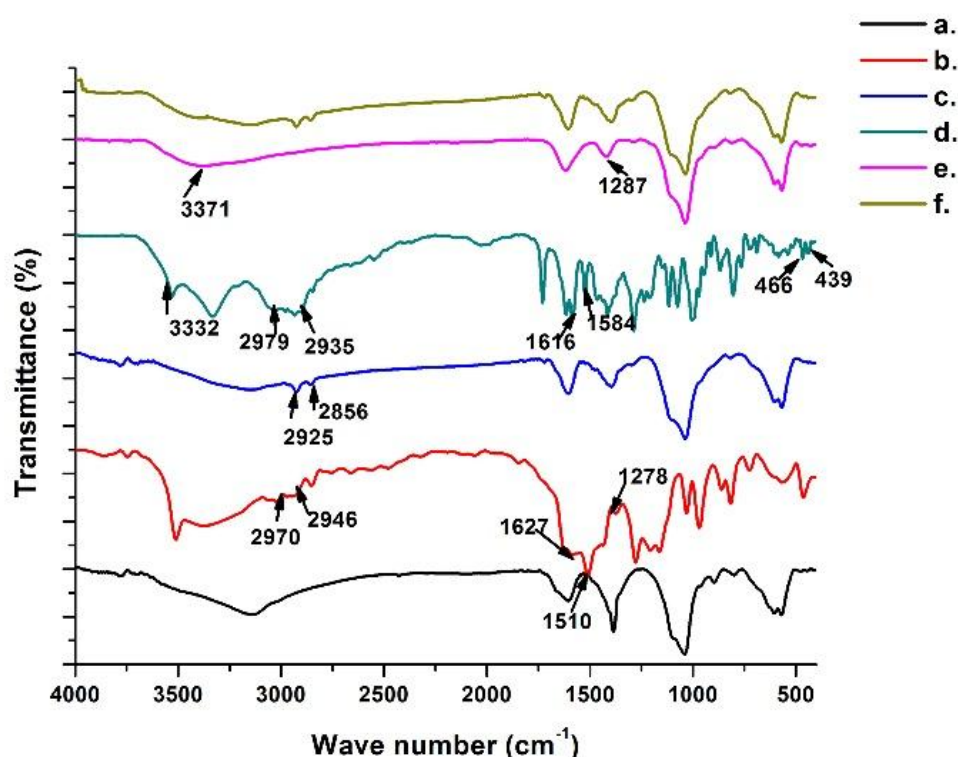


Fig. 1. FT-IR characterization of a) ALG-HI, b) Neat curcumin, c) CR-ALG-HI, d) Neat doxorubicin, e) DX-ALG-HI, f) DX.CR-ALG-HI

As given in Table S1-S4 and Fig. S3-S7., the XPS data clearly indicated that when drug molecules interact with the carrier it leads to the shift of the position of the peaks corresponding to Ca, Fe, P, N, C and O atoms.

The morphological observations were taken by SEM and TEM images which are given in Fig. 2. It is clear that the nanoparticles are aggregated, and discrete particles are hard to distinguish in the SEM images. TEM data show the average size of the neat carrier to be about 13 - 17 nm. The sizes of the CR-ALG-HI, DX-ALG-HI and DX.CR-ALG-HI are larger at 23.4 ± 5.1 nm, 20.6 ± 3.4 nm and 34 ± 5.2 nm respectively. In all the systems, the obtained nanoparticles are well below 50 nm, suggesting they will have the ability to be internalized into cells and progress to the nucleus via the enhanced permeation retention (EPR) effect[49].

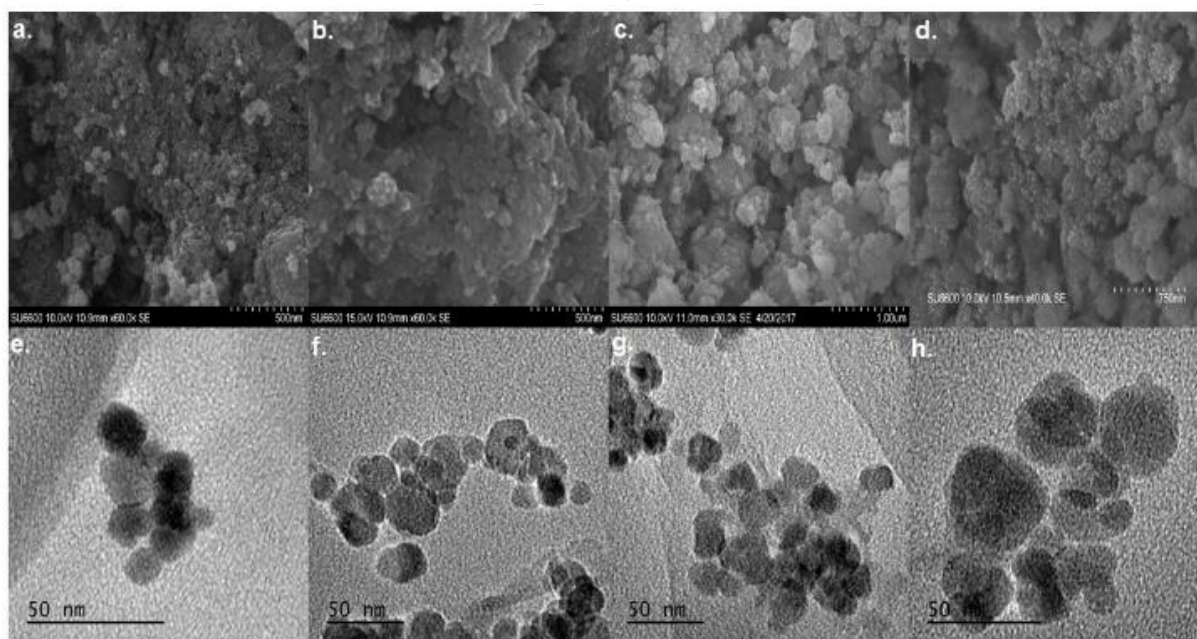


Fig. 2. SEM and TEM images a) SEM image of neat carrier, b) SEM image of CR-ALG-HI, c) SEM image of DX-ALG-HI, d) SEM image of DX.CR-ALG-HI, e) TEM image of neat carrier, f) TEM image of CR-ALG-HI, g) TEM image of DX-ALG-HI and h) TEM image of DX.CR-ALG-HI

3.2. Assessment of drug loading capacity and encapsulation efficiency

The drug loading capacities (DL) and the encapsulation efficiencies (EE) are given in Table S5. It could be seen that these systems have different values for those two parameters and both DL% and EE% of the co-loaded system are lower than the individual drug loaded systems.

3.3. Drug release

The drug release profiles are given in Fig. 3. The neat drug showed a burst of release within a very short time independent of pH. However, the release of drugs from the ALG-HI drug carrier showed a dependency on pH (higher content at lower pH). In the release patterns of both drugs from their carriers, there was an initial burst release within the first 5-6 hours which was then followed sustained release pattern over a period of 168 hours. Such a burst release can be attributed to the release of the surface adsorbed drug molecules[9]. The subsequent slow release can be attributed to favorable interactions between the drug molecules and carrier through electrostatic, van der Waals forces and hydrogen bonding[28].

The released drug content from each system is tabulated in Table S6. However, in both cases it could be seen that the released drug content is higher in singly loaded system than their co-loaded systems.

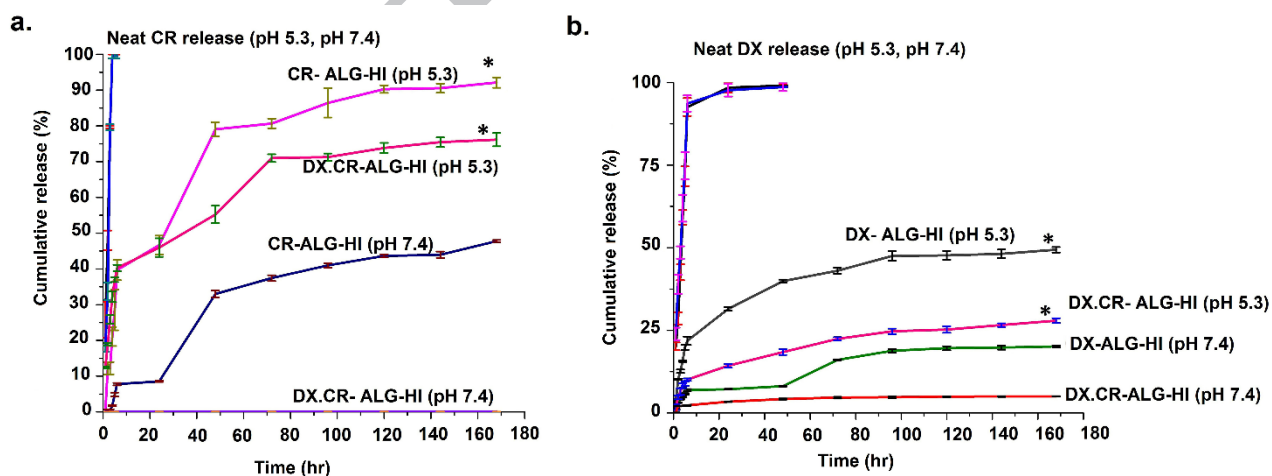


Fig. 3. Cumulative drug release percentage of each drug from the drug carrier system under pH 7.4 and 5.3; a) Release of curcumin with and without the drug carrier at two pH environments, b) Release of doxorubicin with and without drug carrier at two pH environments Results are presented as mean \pm SD, n = 3.

With respect to the curcumin, the doxorubicin cumulative release content is significantly lower ($P < 0.05$), which could be due to the favorable interactions that are formed in between the negatively charged centers of ALG-HI and the positively charged doxorubicin ions or the Vander Waals interactions that are formed between the polysaccharide hexagons in the carrier and the doxorubicin[50].

The advantage of the drug delivery system prepared in this work are thus clear; it is capable of performing sustained and pH sensitive drug release. This may be facilitated by the “open-close gate mechanism mediated by CTAB molecules[28] and the gradual dissolution of HAp coating material[51]. The system particularly promising for the treatment cancer as the drugs are more rapidly released at a lower pH, typical of the cancer microenvironment [28].

3.4. In-vitro cytotoxicity

The dose response and time response curves for the two cell lines are given in Fig. 4, Fig. 5, Fig. S8 and Fig. S8. It is clearly observed that the drug loaded ALG-HI have much more profound time controlled cell disruption ability than the neat drug molecules. This is expected to be due to the controlled release of drug molecules from the nanocarrier, in contrast to the rapid release seen in neat drugs. By such a mechanism, the formulations maintain a prolonged anti-proliferative effect which would minimize the requirement for repeated dosages.

Similarly, when considering the IC₅₀ values of each formulation (Table S7) over MCF-7 breast cancer cells and HEPG2 hepatocellular carcinoma cells, it is clearly evidenced that these values are much lower than the IC₅₀ values of curcumin and doxorubicin alone. The CR-ALG-HI system has significantly lower IC₅₀ values ($P < 0.05$) than the neat drug at all three time points. Furthermore, compared with the literature, the IC₅₀ values reported for the CR-ALG-HI in our study is remarkably low highlighting its potency over both cell types[22],[52],[53].

A similar trend has been exerted by the DX- ALG-HI with very low IC₅₀ values. These values are promising when compared to the reported work[54],[55]. Compared to the CR-ALG-HI and DX-

ALG-HI the combined system is no more effective with MCF-7 cells than the single-drug systems. However, with respect to neat curcumin and doxorubicin, the IC₅₀ values of the co-loaded system are much lower. More importantly our systems have much lower IC₅₀ values than have been reported in the literature for curcumin/doxorubicin combined treatment of breast and liver cancer[9],[22],[25]. With the HEPG2 cells the co-loaded system performs even better than the single-drug analogue or the neat drugs, resulting in lower IC₅₀ values. This could be due to the synergistic effect[4] created by curcumin molecules over the activity of doxorubicin, and this combinational effect is much profound on HEPG2 cells. The increase in glutathione (GSH) levels is generally a key factor leading to resistance in chemotherapy or radiotherapy [56]. However, it has been found that HEPG2 cells have very high levels of intrinsic GSH[56] rendering for higher IC₅₀ dosages. Therefore, the co-delivery of both curcumin and doxorubicin via this drug carrier might have accounted favorably for the reduction of GSH levels and thereby requiring low IC₅₀ to provide the effect.

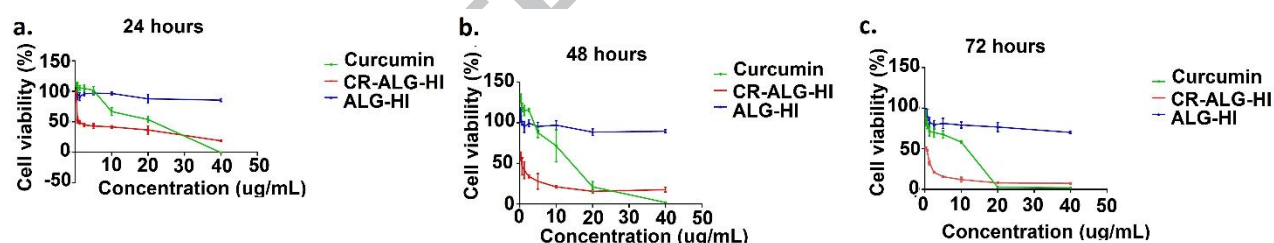


Fig. 4. Dose responsive and time response curves of MCF 7 cells treated with ALG-HI, Curcumin and CR-ALG-HI a) after 24 hours, b) after 48 hours and c) after 72 hours. Results are presented as mean \pm SD, from three independent experiments each containing three replicates.

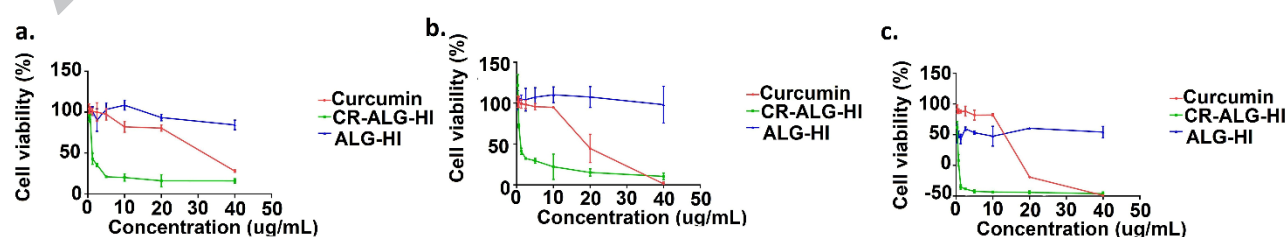


Fig. 5. Dose responsive and time responsive curves of HEPG2 cells treated with ALG-HI, curcumin and CR-ALG-HI a) after 24 hours, b) after 48 hours, c) after 72 hours. Results are presented as mean \pm SD, from three independent experiments each containing three replicates.

3.5. Fluorescence imaging

Fig. 6,7 and Fig. S10- Fig. S12 depict phase contrast images and fluorescence images of cells that have been treated with the nanoparticles for 24, 48 and 72-hours. It is clearly visible that the control cells have maintained the fusiform shape while being uniformly stained in green (AO/EB staining) and blue (Hoechst staining), showing them to be healthy[57]. However, as shown in Fig. 6. a. b. and Fig. S10, when both MCF-7 cells and HEPG2 cells are treated by curcumin, they have started to undergo apoptosis, expressing bright yellow to orange nuclei with AO/EB staining and medium to bright blue color with Hoechst staining. Further, the cells have shrunk and appeared in an irregular shape[58]. The cell number reduce with time, as cells have undergone death and been removed with the washing steps. This effect is much more profound with the CR- ALG-HI treated systems as it has led to the appearance of more round shaped cells and bright nuclei due to the chromatin condensation and nuclear fragmentation[58]. Most of the cells have lost cell integrity and have not stained well with Hoechst[57].

Similar observations can be made with doxorubicin and the doxorubicin loaded nanoparticles, as given in Fig. 7. and Fig. S11, S12. More specifically it is obvious that the apoptotic effect is much stronger with these systems than with curcumin, confirming the potency of doxorubicin and their lower IC50 values. The dual drug loaded materials (Fig. S13. a, b) are much effective against HEPG2 cells than MCF-7 cells, as was noted previously.

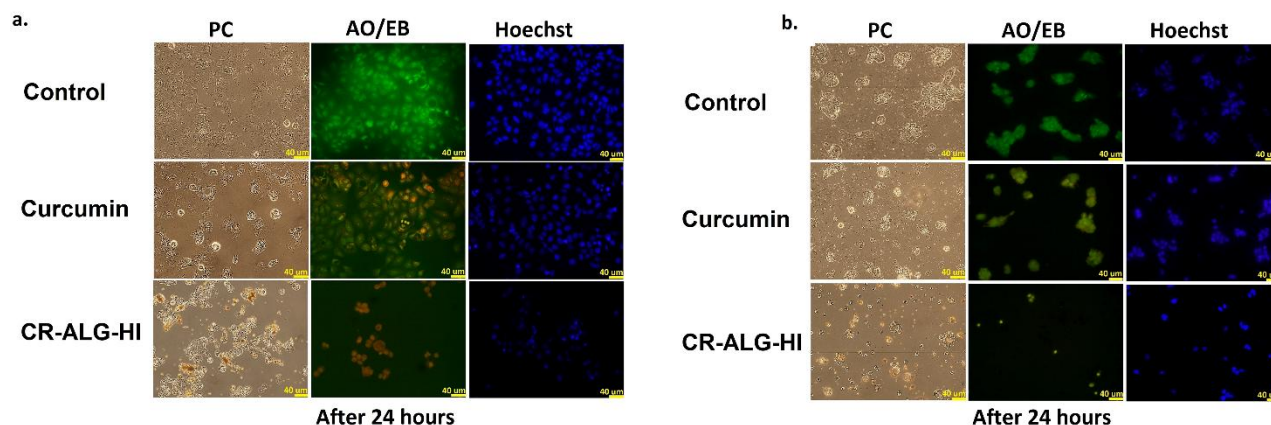


Fig. 6. Phase contrast (PC) and fluorescence images obtained to assess the effect of curcumin and CR-ALG-HI on the a) MCF-7 cells, b) HEPG2 cells incubated for 24 hours. Scale bar is 40 μm

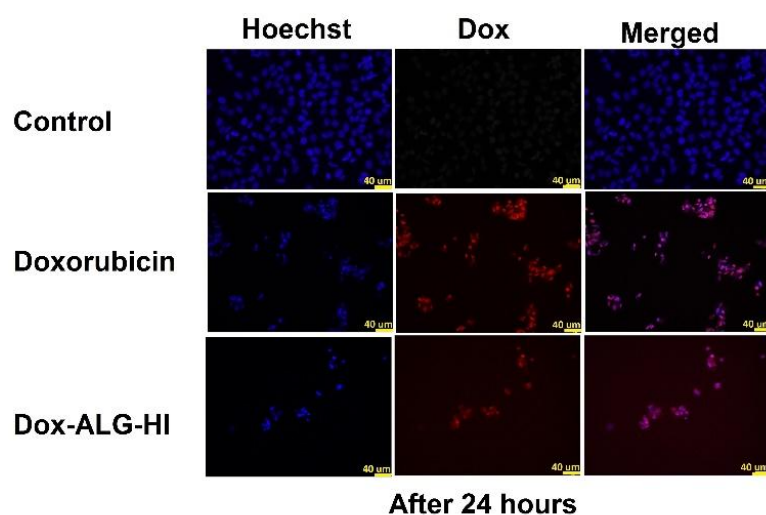


Fig. 7. Phase contrast (PC) and fluorescence images obtained to assess the effect of doxorubicin and DX-ALG-HI on the a) MCF-7 cells for 24 hours. Scale bar is 40 μm.

3.6. Flow cytometry

The results of staining to quantify live/apoptotic/late apoptotic and dead cells are given in Fig. 8. and Fig. S14. These reveal that, compared to the neat drug molecules, drug loaded ALG-HI show a higher percentage of cells lying in the late apoptotic and necrotic or dead stages. This is common to all the NP systems. Compared to HEPG2 cells, apoptotic induction in MCF-7 is greater. MCF-7 cells have apoptotic or dead cells at $23.95 \pm 0.89\%$, $42.56 \pm 0.34\%$ and $39.05 \pm 0.45\%$ when incubated

with CR-ALG-HI, DX- ALG-HI and with DX.CR- ALG-HI respectively. Similarly, in HEpG2 cells a significant percentage ($P < 0.05$) of cells undergoing apoptosis and necrosis could be seen with cells treated with CR-ALG-HI, DX-ALG-HI and DX.CR-ALG-HI materials ($67.01 \pm 0.55\%$, $21.62 \pm 0.67\%$, $49.55 \pm 0.35\%$) with respect to the control and the neat drug treatment. This has further highlighted that the apoptotic induction ability of these systems are far superior than the neat drug doxorubicin and therefore could be used as a replacement for the toxic doxorubicin.

In general, this remarkable apoptosis induction ability of the drug loaded nanoparticles could arise due to the higher uptake of the nanoparticles and the diffusion of more drug molecules into the nucleus [59],[60]. The histograms of single stains (Cells with Annexin V and Cells with ZG stained separately) used as compensation controls are given in Fig. S15.

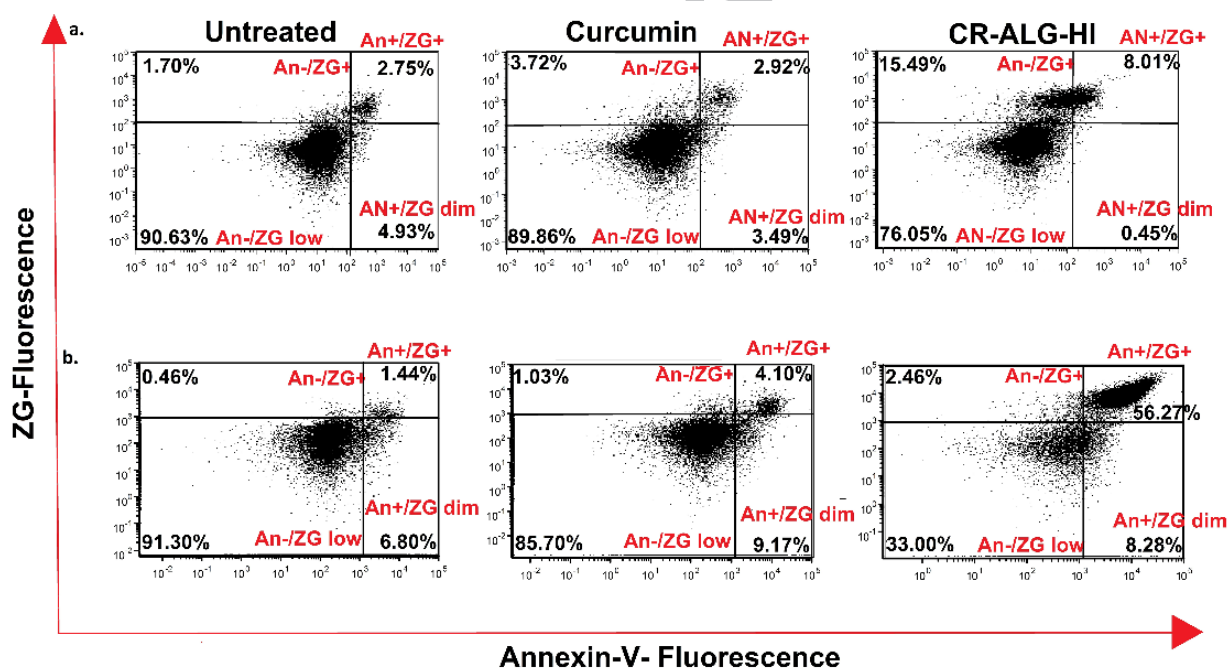


Fig. 8 Flow cytometric analysis of apoptotic induction of a) MCF-7 and b) HEpG2 cells by drugs and drug bound nanoparticles after staining with Annexin V- APC abbreviated as (AN) for ease of labelling /Zombie green (ZG). AN-/ZG+, necrotic or debris cells; AN+/ZG+, late apoptotic cells; AN-/ZG low, viable; AN+/ZG dim, apoptotic cells. Numbers in each quadrant represent the

percentage of cells (data are representative of mean \pm SD of triplicated of three individual experiments)

3.7. Assessment of hemocompatibility, bone marrow proliferation and effect on non-cancerous cells

As given in Fig. S16. a. and b., low hemolytic percentages well below 1.5%, suggest the hemocompatibility of the nanoparticles. These values are very low compared with the reported work on these drugs and similar drug loaded nanoparticles[19],[61]. All the drug loaded nanoparticles are critically safe to be used for cancer treatment, as recommended by ISO/TR 7406 [61].

The effect of the curcumin, doxorubicin, CR-ALG-HI, DX-ALG-HI and DX.CR-ALG-HI on the cell proliferation of rat bone marrow cells (Fig. S17) implied that both ALG-HI nanoparticle and drug bound ALG-HI systems maintained a very good cell viability even at high concentrations. Thus, the drug loaded nanoparticle systems do not induce adverse effects on bone marrow cells, demonstrating their increased biocompatibility which might arise due to the inherent properties of the ALG-HI such as HAp, NaAlg and IONPs[42].

From the cytotoxicity results on non-cancerous Vero cells as depicted in Fig. S18. a, b and c., it is clear that there are differences in how cancerous and non-cancerous cells respond to the formulations. The viability of the Vero cells is generally high, with the NPs performing significantly better than the free drug in this regard. Given that the IC₅₀ values obtained for the drug loaded nanoparticles over MCF-7 and HEPG2 cells are very much lower compared to the reported work it appears that these formulations are much safer for therapeutic use than the pure drugs. The cytotoxic effects caused by our nanoparticles on Vero cells are very low when compared with the reported work carried out using carbon nanotubes (CNTs) and Al₂O₃ nanoparticles [62],[63].

4. Conclusions

A drug carrier comprised of a magnetic core with HAp shell was successfully synthesized and loaded with curcumin, doxorubicin and a combination of the two in this work. Efficient loading was

observed, and the release of the drugs as was pH sensitive, with faster release in the mildly acidic conditions typical of the cancer microenvironment. Extended release over around one week was observed. Anti-proliferative studies have proven that CR-ALG-HI, DX-ALG-HI and the dual drug loaded ALG-HI are very potent, with lower IC₅₀ values against breast and liver cancer cells than the free drug molecules. Fluorescence imaging and flow cytometry reveals that this is due to the greater extent of apoptosis induced by the drug loaded nanoparticles. Hemolysis tests, cytotoxic evaluation on bone marrow cells and green monkey kidney epithelial cells verified that the nanoparticle systems are devoid of adverse side effects, and cause selective toxicity to cancer cells while leaving healthy cells unaffected. The drug loaded nanoparticles reported here could potentially minimize the amount of doxorubicin or curcumin required for effective therapeutic action, ensuring the minimization of any possible side effect.

Acknowledgements

Authors like to extend the sincere gratitude to National Research Council Sri Lanka (NRC 14-016) for the financial support provided. The authors are also grateful for the science team at SLINTEC, technical officers at Department of Chemistry, University of Colombo and Faculty of Medical Sciences, University of Sri Jayewardenepura for the necessary support provided during the characterization purposes.

References

- [1] US. Breast Cancer Statistics, http://www.breastcancer.org/symptoms/understand_bc/statistics, (assessed September 2017).
- [2] Y. Zhao, Q. Ju, G. Li, Tumor markers for hepatocellular carcinoma (Review), *Mol Clin Oncol.* (2013) 593–598. doi:10.3892/mco.2013.119.
- [3] American Cancer Society, <https://www.cancer.org/cancer/liver-cancer/about/what-is-key-statistics.html>, (assessed September 2017).

- [4] A. Florea, D. Büsselberg, Cisplatin as an anti-tumor drug: cellular mechanisms of activity, drug resistance and induced side effects, *Cancers (Basel)*. (2011) 2315–2325. doi:10.1039/B820550G.
- [5] J. Varshosaz, M. Farzan, Advances in Hepatocellular Carcinoma Nanoparticles for targeted delivery of therapeutics and small interfering RNAs in hepatocellular carcinoma, *World J Gastroenterol*. 21 (2015) 12022–12041. doi:10.3748/wjg.v21.i42.12022.
- [6] S.K. Sriraman, G. Salzano, C. Sarisozen, V. Torchilin, Anti-cancer activity of doxorubicin-loaded liposomes co-modified with transferrin and folic acid, *Eur. J. Pharm. Biopharm.* 105 (2016) 40–49. doi:10.1016/j.ejpb.2016.05.023.
- [7] A. Mohan, S. Narayanan, G. Balasubramanian, S. Sethuraman, U.M. Krishnan, Dual drug loaded nanoliposomal chemotherapy: A promising strategy for treatment of head and neck squamous cell carcinoma, *Eur. J. Pharm. Biopharm.* 99 (2016) 73–83. doi:10.1016/j.ejpb.2015.11.017.
- [8] M.E.R. O'Brien, N. Wigler, M. Inbar, R. Rosso, E. Grischke, A. Santoro, R. Catane, D.G. Kieback, P. Tomczak, S.P. Ackland, F. Orlandi, L. Mellars, L. Alland, C. Tendler, Reduced cardiotoxicity and comparable efficacy in a phase III trial of pegylated liposomal doxorubicin HCl (CAELYX™/Doxil®) versus conventional doxorubicin for first-line treatment of metastatic breast cancer, *Ann. Oncol.* 15 (2004) 440–449. doi:10.1093/annonc/mdh097.
- [9] X. Zhao, Q. Chen, W. Liu, Y. Li, H. Tang, X. Liu, X. Yang, Codelivery of doxorubicin and curcumin with lipid nanoparticles results in improved efficacy of chemotherapy in liver cancer, *Int. J. Nanomedicine*. 10 (2014) 257–270. doi:10.2147/IJN.S73322.
- [10] S. Rivankar, An overview of doxorubicin formulations in cancer therapy, *J. Cancer Res. Ther.* 10 (2014) 853. doi:10.4103/0973-1482.139267.
- [11] J.M. Saul, A. Annapragada, J. V. Natarajan, R. V. Bellamkonda, Controlled targeting of liposomal doxorubicin via the folate receptor in vitro, *J. Control. Release*. 92 (2003) 49–67. doi:10.1016/S0168-3659(03)00295-5.

- [12] B. Zhu, H. Zhang, L. Yu, Novel transferrin modified and doxorubicin loaded Pluronic 85/lipid-polymeric nanoparticles for the treatment of leukemia: In vitro and in vivo therapeutic effect evaluation, *Biomed. Pharmacother.* 86 (2017) 547–554. doi:10.1016/j.biopha.2016.11.121.
- [13] B. Kundu, D. Ghosh, M.K. Sinha, P.S. Sen, V.K. Balla, N. Das, D. Basu, Doxorubicin-intercalated nano-hydroxyapatite drug-delivery system for liver cancer: An animal model, *Ceram. Int.* 39 (2013) 9557–9566. doi:10.1016/j.ceramint.2013.05.074.
- [14] M. Itokazu, S. Kumazawa, E. Wada, Y. Wenyi, Sustained release of adriamycin from implanted hydroxyapatite block for the treatment of experimental osteogenic sarcoma in mice, *Cancer Lett.* 107 (1996) 11–18. doi: 10.1016/0304-3835(96)04337-6
- [15] O. Vittorio, M. Le Grand, S.A. Makharza, M. Curcio, P. Tucci, F. Iemma, F.P. Nicoletta, S. Hampel, G. Cirillo, Doxorubicin synergism and resistance reversal in human neuroblastoma BE(2)C cell lines: An in vitro study with dextran-catechin nano hybrids, *Eur. J. Pharm. Biopharm.* 122 (2018) 176–185. doi:10.1016/j.ejpb.2017.11.005.
- [16] X. Su, Z. Wang, L. Li, M. Zheng, C. Zheng, P. Gong, P. Zhao, Y. Ma, Q. Tao, L. Cai, Lipid-polymer nanoparticles encapsulating doxorubicin and 2'-deoxy-5-azacytidine enhance the sensitivity of cancer cells to chemical therapeutics, *Mol. Pharm.* 10 (2013) 1901–1909. doi:10.1021/mp300675c.
- [17] S. Li, D. Amat, Z. Peng, S. Vanni, S. Raskin, G. De Angulo, A.M. Othman, R.M. Graham, R.M. Leblanc, *Nanoscale.* 30 (2016) 147–154. doi:10.1039/C6NR05055G.
- [18] S. Mancarella, V. Greco, F. Baldassarre, D. Vergara, M. Maffia, S. Leporatti, Polymer-Coated Magnetic Nanoparticles for Curcumin Delivery to Cancer Cells, *Macromol. Biosci.* 15 (2015) 1365–1374. doi:10.1002/mabi.201500142.
- [19] M. Akrami, M. Khoobi, M. Khalilvand-Sedagheh, I. Haririan, A. Bahador, M.A. Faramarzi, S. Rezaei, H.A. Javar, F. Salehi, S.K. Ardestani, A. Shafiee, Evaluation of multilayer coated

magnetic nanoparticles as biocompatible curcumin delivery platforms for breast cancer treatment, *RSC Adv.* 5 (2015) 88096–88107. doi:10.1039/C5RA13838H.

[20] C.Y.H. A.L. Cheng, C. H. Hsu, J. K. Lin, M. M. Hsu, Y. F. Ho, T. S. Shen, J. Y. Ko, J. T. Lin, B. R. Lin, M. S. Wu, H. S. Yu, S. H. Jee, G. S. Chen, T. M. Chen, C. A. Chen, M. K. Lai, Y. S. Pu, M. S. Pan, Y. J. Wang, C. C. Tsai, Phase I clinical trial of curcumin , a chemo preventive agent , in patients with high- risk or pre-malignant lesions, *Anticancer Res.* 21 (2001) 2895–2900.

[21] J. Duan, H.M. Mansour, Y. Zhang, X. Deng, Y. Chen, J. Wang, Y. Pan, J. Zhao, Reversion of multidrug resistance by co-encapsulation of doxorubicin and curcumin in chitosan/poly(butyl cyanoacrylate) nanoparticles, *Int. J. Pharm.* 426 (2012) 193–201. doi:10.1016/j.ijpharm.2012.01.020.

[22] L. Sun, X. Deng, X. Yang, Z. Li, Z. Wang, L. Li, Q. Wu, F. Peng, L. Liu, C. Gong, Co-delivery of doxorubicin and curcumin by polymeric micelles for improving antitumor efficacy on breast carcinoma, *RSC Adv.* 4 (2014) 46737–46750. doi:10.1039/C4RA07453J.

[23] N. Ghalandarlaki, A.M. Alizadeh, S. Ashkani-Esfahani, Nanotechnology-applied curcumin for different diseases therapy, *Biomed Res. Int.* 2014 (2014). doi:10.1155/2014/394264.

[24] L. Hosseinzadeh, J. Behravan, F. Mosaffa, G. Bahrami, A.R. Bahrami, G. Karimi, Effect of curcumin on doxorubicin-induced cytotoxicity in h9c2 cardiomyoblast cells, *Iran. J. Basic Med. Sci.* 14 (2011) 49-56. doi:10.22038/IJBMS.2011.4964.

[25] T. Cui, Z. Sihao, H. Sun, Co-delivery of doxorubicin and pH-sensitive curcumin prodrug by transferrin-targeted nanoparticles for breast cancer treatment, *Oncol. Rep.* 37 (2017) 1253–1260. doi:10.3892/or.2017.5345.

[26] H. Xiong, S. Du, J. Ni, J. Zhou, J. Yao, Mitochondria and nuclei dual-targeted heterogeneous hydroxyapatite nanoparticles for enhancing therapeutic efficacy of doxorubicin, *Biomaterials.* 94 (2016) 70–83. doi:10.1016/j.biomaterials.2016.04.004.

- [27] A. Pistone, D. Iannazzo, S. Panseri, M. Montesi, A. Tampieri, S. Galvagno, Hydroxyapatite-magnetite-MWCNT nanocomposite as a biocompatible multifunctional drug delivery system for bone tissue engineering, *Nanotechnology*. 25 (2014) 425701. doi:10.1088/0957-4484/25/42/425701.
- [28] D.C. Manatunga, R.M. de Silva, K.M.N. de Silva, N. de Silva, S. Bhandari, Y.K. Yap, N.P. Costha, pH responsive controlled release of anti-cancer hydrophobic drugs from sodium alginate and hydroxyapatite bi-coated iron oxide nanoparticles, *Eur. J. Pharm. Biopharm.* 117 (2017) 29–38. doi:10.1016/j.ejpb.2017.03.014.
- [29] C.H. Hou, S.M. Hou, Y.S. Hsueh, J. Lin, H.C. Wu, F.H. Lin, The in vivo performance of biomagnetic hydroxyapatite nanoparticles in cancer hyperthermia therapy, *Biomaterials*. 30 (2009) 3956–3960. doi:10.1016/j.biomaterials.2009.04.020.
- [30] S. Panseri, C. Cunha, T. D'Alessandro, M. Sandri, A. Russo, G. Giavaresi, M. Marcacci, C.T. Hung, A. Tampieri, Magnetic Hydroxyapatite bone substitutes to enhance tissue regeneration: Evaluation in vitro using osteoblast-like cells and in vivo in a bone defect, *PLoS One*. 7 (2012) 4–11. doi:10.1371/journal.pone.0038710.
- [31] K.M. Laginha, S. Verwoert, G.J.R. Charrois, T.M. Allen, Determination of doxorubicin levels in whole tumor and tumor nuclei in murine breast cancer tumors, *Clin. Cancer Res.* 11 (2005) 6944–6949. doi:10.1158/1078-0432.CCR-05-0343.
- [32] J. Li, I.W. Lee, G.H. Shin, X. Chen, H.J. Park, Curcumin- Eudragit® E PO solid dispersion: A simple and potent method to solve the problems of curcumin, *Eur J Pharm Biopharm.* 94 (2015) 322-332. doi:10.1016/j.ejpb.2015.06.002.
- [33] X.Z. Zhang, D.Q. Wu, C.C. Chu, Synthesis, characterization and controlled drug release of thermosensitive IPN-PNIPAAm hydrogels, *Biomaterials*. 25 (2004) 3793–3805. doi:10.1016/j.biomaterials.2003.10.065.

- [34] G. Turkmen, A. K., Cavalu, S., Goller, Development of Chitosan-Hydroxyapatite- Fibrinogen 3D Scaffolds For Bone Tissue Regeneration Development of Chitosan-Hydroxyapatite-Fibrinogen 3D Scaffolds For Bone Tissue Regeneration, *J. Aust. Cermain Soc.* 52 (2016) 34–41.
- [35] N. Sanoj Rejinold, M. Muthunarayanan, V. V. Divyarani, P.R. Sreerekha, K.P. Chennazhi, S. V. Nair, H. Tamura, R. Jayakumar, Curcumin-loaded biocompatible thermoresponsive polymeric nanoparticles for cancer drug delivery, *J. Colloid Interface Sci.* 360 (2011) 39–51. doi:10.1016/j.jcis.2011.04.006.
- [36] B. Wu, S.T. Lu, L.J. Zhang, R.X. Zhuo, H.B. Xu, S.W. Huang, Codelivery of doxorubicin and triptolide with reduction-sensitive lipid–polymer hybrid nanoparticles for in vitro and in vivo synergistic cancer treatment, *Int. J. Nanomedicine.* 12 (2017) 1853–1862. doi:10.2147/IJN.S131235.
- [37] S. Selim, S. Al Jaouni, Anticancer and apoptotic effects on cell proliferation of diosgenin isolated from *Costus speciosus* (Koen.) Sm., *BMC Complement. Altern. Med.* 15 (2015) 301. doi:10.1186/s12906-015-0836-8.
- [38] J. Monga, S. Pandit, R.S. Chauhan, C.S. Chauhan, S.S. Chauhan, M. Sharma, Growth Inhibition and Apoptosis Induction by (+)-Cyanidan-3-ol in Hepatocellular Carcinoma, *PLoS One.* 8 (2013) 1–19. doi:10.1371/journal.pone.0068710.
- [39] I. Mottas, A. Milosevic, A. Petri-Fink, B. Rothen-Rutishauser, C. Bourquin, *Nanoscale.* 1 (2017) 10–29. doi:10.1039/C6NR08194K.
- [40] A. Persidis, Cancer multidrug resistance., *Nat. Biotechnol.* 17 (1999) 94–95. doi:10.1038/80051.
- [41] J.-S. Kim, J. Shin, S. Ko, A. Cristina, S. Samia, Characterization, Quantification, and Determination of the Toxicity of Iron Oxide Nanoparticles to the Bone Marrow Cells Sae-Yeol-Rim Paik, *Int. J. Mol. Sci.* 16 (2015) 22243–22257. doi:10.3390/ijms160922243.
- [42] N.S. Remya, S. Syama, V. Gayathri, H.K. Varma, P. V. Mohanan, An in vitro study on the interaction of hydroxyapatite nanoparticles and bone marrow mesenchymal stem cells for assessing

the toxicological behaviour, *Colloids Surfaces B Biointerfaces*. 117 (2014) 389–397. doi:10.1016/j.colsurfb.2014.02.004.

[43] M.L. Mojica Piscioti, E. Lima, M. Vasquez Mansilla, V.E. Tognoli, H.E. Troiani, A.A. Pasa, T.B. Creczynski-Pasa, A.H. Silva, P. Gurman, L. Colombo, G.F. Goya, A. Lamagna, R.D. Zysler, In vitro and in vivo experiments with iron oxide nanoparticles functionalized with DEXTRAN or polyethylene glycol for medical applications: Magnetic targeting, *J. Biomed. Mater. Res. - Part B Appl. Biomater.* 102 (2014) 860–868. doi:10.1002/jbm.b.33068.

[44] K. Muthoosamy, I.B. Abubakar, R.G. Bai, H.-S. Loh, S. Manickam, Exceedingly Higher co-loading of Curcumin and Paclitaxel onto Polymer-functionalized Reduced Graphene Oxide for Highly Potent Synergistic Anticancer Treatment., *Sci. Rep.* 6 (2016) 32808. doi:10.1038/srep32808.

[45] C. Yucel, V. Quagliariello, R.V. Iaffaioli, G. Ferrari, F. Donsi, Submicron complex lipid carriers for curcumin delivery to intestinal epithelial cells: Effect of different emulsifiers on bioaccessibility and cell uptake, *Int. J. Pharm.* 494 (2015) 357–369. doi:10.1016/j.ijpharm.2015.08.039.

[46] R.A. Campbell, S.R.W. Parker, J.P.R. Day, C.D. Bain, External reflection FTIR spectroscopy of the cationic surfactant hexadecyltrimethylammonium bromide (CTAB) on an overflowing cylinder, *Langmuir*. 20 (2004) 8740–8753. doi:10.1021/la048680x.

[47] G.T. Usca, C.V. Gómez, D.C. Fiallos, P. Tavolaro, G. Martino, L.S. Caputi, A. Tavolaro, Preparation of graphene oxide as biomaterials for drug adsorption, *AIP Conf. Proc.* 1646 (2015) 79–86. doi:10.1063/1.4908586.

[48] M. Wójcik, W. Lewandowski, M. Król, K. Pawłowski, J. Mieczkowski, R. Lechowski, K. Zabielska, Enhancing anti-tumor efficacy of doxorubicin by non-covalent conjugation to gold nanoparticles - In vitro studies on Feline fibrosarcoma cell lines, *PLoS One*. 10 (2015) 1–15. doi:10.1371/journal.pone.0124955.

- [49] L. Lv, K. Qiu, X. Yu, C. Chen, F. Qin, Y. Shi, J. Ou, T. Zhang, H. Zhu, J. Wu, C. Liu, G. Li, Amphiphilic copolymeric micelles for doxorubicin and curcumin co-delivery to reverse multidrug resistance in breast cancer, *J. Biomed. Nanotechnol.* 12 (2016) 973–985. doi:10.1166/jbn.2016.2231.
- [50] R. Dinarvand, N. Sepehri, S. Manoochehri, H. Rouhani, F. Atyabi, Polylactide-co-glycolide nanoparticles for controlled delivery of anticancer agents., *Int. J. Nanomedicine.* 6 (2011) 877–895. doi:10.2147/IJN.S18905.
- [51] F. Chen, C. Li, Y.-J. Zhu, X.-Y. Zhao, B.-Q. Lu, J. Wu, Magnetic nanocomposite of hydroxyapatite ultrathin nanosheets/Fe₃O₄ nanoparticles: Microwave-assisted rapid synthesis and application in pH-responsive drug release, *Biomater. Sci.* 1 (2013) 1074–1081. doi:10.1039/c3bm60086f.
- [52] Z. Liu, Y. Sun, L. Ren, Y. Huang, Y. Cai, Q. Weng, X. Shen, X. Li, G. Liang, Y. Wang, Evaluation of a curcumin analog as an anti-cancer agent inducing ER stress-mediated apoptosis in non-small cell lung cancer cells., *BMC Cancer.* 13 (2013) 494. doi:10.1186/1471-2407-13-494.
- [53] B. Strojny, M. Grodzik, E. Sawosz, A. Winnicka, N. Kurantowicz, S. Jaworski, M. Kutwin, K. Urbańska, A. Hotowy, M. Wierzbicki, A. Chwalibog, Diamond nanoparticles modify curcumin activity: In vitro studies on cancer and normal cells and in ovo studies on chicken embryo model, *PLoS One.* 11 (2016) 1–18. doi:10.1371/journal.pone.0164637.
- [54] K. Polakova, K. Polakova, K. Pizova, S. Binder, M. Havrdova, M. Kolarova, E. Kriegova, J. Zapletalova, L. Malina, J. Horakova, J. Malohlava, A. Kolokithas-Ntoukas, A. Bakandritsos, H. Kolarova, R. Zboril, In vitro cytotoxicity analysis of doxorubicin-loaded/superparamagnetic iron oxide colloidal nanoassemblies on MCF7 and NIH3T3 cell lines, *Int. J. Nanomedicine.* 10 (2015) 949–961. doi:10.2147/IJN.S72590.
- [55] F.A. Langroodi, Evaluation of the effect of crocetin on antitumor activity of doxorubicin encapsulated in PLGA nanoparticles, *Nanomed J.* 3 (2016) 23–34. doi:10.7508/nmj.2016.01.003.

- [56] C. Syng-ai, a L. Kumari, A. Khar, C. Syng-ai, a L. Kumari, Effect of curcumin on normal and tumor cells : Role of glutathione and bcl-2 Effect of curcumin on normal and tumor cells : Role of glutathione and bcl-2, *Mol Cancer Ther.* 3 (2004) 1101–1108.
- [57] G. Varbiro, Enhancement of the Cytotoxic Effect of Anticancer Agent by Cytochrome c Functionalised Hybrid Nanoparticles in Hepatocellular Cancer Cells, *J. Nanomedicine Res.* 1 (2014) 1–8. doi:10.15406/jnmr.2014.01.00010.
- [58] R. Thangam, M. Sathuvan, A. Poongodi, V. Suresh, K. Pazhanichamy, S. Sivasubramanian, N. Kanipandian, N. Ganesan, R. Rengasamy, R. Thirumurugan, S. Kannan, Activation of intrinsic apoptotic signaling pathway in cancer cells by *Cymbopogon citratus* polysaccharide fractions, *Carbohydr. Polym.* 107 (2014) 138–150. doi:10.1016/j.carbpol.2014.02.039.
- [59] A. Anitha, S. Maya, N. Deepa, K.P. Chennazhi, S. V. Nair, H. Tamura, R. Jayakumar, Efficient water soluble O-carboxymethyl chitosan nanocarrier for the delivery of curcumin to cancer cells, *Carbohydr. Polym.* 83 (2011) 452–461. doi:10.1016/j.carbpol.2010.08.008.
- [60] S. Ahn, E. Seo, K. Kim, S.J. Lee, Controlled cellular uptake and drug efficacy of nanotherapeutics., *Sci. Rep.* 3 (2013)1-10. doi:10.1038/srep01997.
- [61] V. Rajiu, P. Balaji, T.S. Sheena, M.A. Akbarsha, K. Jeganathan, Doxorubicin-Anchored Curcumin Nanoparticles for Multimode Cancer Treatment against Human Liver Carcinoma Cells, *Part. Part. Syst. Charact.* 32 (2015) 1–15. doi:10.1002/ppsc.201500098.
- [62] F.A. Prakash, G.J.D. Babu, M. Lavanya, Toxicity Studies of Aluminium Oxide Nanoparticles in Cell Lines, *Int. J. Nanotechnol. Appl.* 5 (2011) 99–107.
- [63] M. Dekaliuk, K. Pyrshev, A. Demchenko, Visualization and detection of live and apoptotic cells with fluorescent carbon nanoparticles, *J. Nanobiotechnology.* 13 (2015) 86. doi:10.1186/s12951-015-0148-7.

Graphical abstract

